

## Spin-flip isovector giant resonances from the $^{90}\text{Zr}(n,p)^{90}\text{Y}$ reaction at 198 MeV

K. J. Raywood,<sup>a</sup> B. M. Spicer,<sup>a</sup> S. Yen,<sup>b</sup> S. A. Long,<sup>a</sup> M. A. Moinester,<sup>c</sup> R. Abegg,<sup>b</sup>  
W. P. Alford,<sup>c</sup> A. Celler,<sup>b,d</sup> T. E. Drake,<sup>f</sup> D. Frekers,<sup>b,f</sup> P. E. Green,<sup>b</sup> O. Häusser,<sup>b,d</sup> R. L. Helmer,<sup>b,e</sup>  
R. S. Henderson,<sup>a,b</sup> K. H. Hicks,<sup>b</sup> K. P. Jackson,<sup>b</sup> R. G. Jeppesen,<sup>d</sup> J. D. King,<sup>f</sup>  
N. S. P. King,<sup>g</sup> C. A. Miller,<sup>b</sup> V. C. Officer,<sup>a</sup> R. Schubank,<sup>b,f</sup> G. G. Shute,<sup>a</sup> M. Vetterli,<sup>d</sup>  
J. Watson,<sup>h</sup> and A. I. Yavin<sup>c</sup>

<sup>a</sup>*School of Physics, University of Melbourne, Parkville, Victoria 3052, Australia*

<sup>b</sup>*TRIUMF, 4004 Wesbrook Mall, Vancouver, British Columbia, Canada V6T 2A3*

<sup>c</sup>*School of Physics, Raymond and Beverly Sackler Faculty of Exact Sciences, Tel Aviv University,  
69978 Ramat Aviv, Israel*

<sup>d</sup>*Department of Physics, Simon Fraser University, Burnaby, British Columbia, Canada V5A 1S6*

<sup>e</sup>*Department of Physics, University of Western Ontario, London, Ontario, Canada N6A 3K7*

<sup>f</sup>*Department of Physics, University of Toronto, Toronto, Ontario, Canada M5S 1A7*

<sup>g</sup>*Los Alamos National Laboratory, Los Alamos, New Mexico 87545*

<sup>h</sup>*Department of Physics, Kent State University, Kent, Ohio 44242*

(Received 10 October 1989)

Doubly differential cross sections of the reaction  $^{90}\text{Zr}(n,p)^{90}\text{Y}$  have been measured at 198 MeV for excitations up to 38 MeV in the residual nucleus. An overall resolution of 1.3 MeV was achieved. The spectra show qualitative agreement in shape and magnitude with recent random phase approximation calculations; however, all of the calculations underestimate the high excitation region of the spectra. A multipole decomposition of the data has been performed using differential cross sections calculated in the distorted-wave impulse approximation. An estimate of the Gamow-Teller strength in the reaction is given. The isovector spin-flip dipole giant resonance has been identified and there is also an indication of isovector monopole strength.

### I. INTRODUCTION

The study of nuclear giant resonances began with the discovery of the electric dipole giant resonance in photonuclear reactions by Baldwin and Klaiber<sup>1</sup> and it was described in terms of collective oscillation of protons against neutrons by Goldhaber and Teller.<sup>2</sup> For almost 25 years this remained the only giant resonance known, until the discovery of the isoscalar electric quadrupole giant resonance in inelastic proton scattering by Lewis and Bertrand<sup>3</sup> in 1972, and in inelastic electron scattering by Pitthan and Walcher<sup>4</sup> and by Fukuda and Torizuka.<sup>5</sup> Since then, the isoscalar monopole and octupole giant resonances have been found. A major advance was made with the discovery of the Gamow-Teller giant resonance ( $\Delta L = 0, \Delta S = 1$ ) by Doering *et al.*,<sup>6</sup> and the study of its systematics by Bainum *et al.*<sup>7</sup> and Anderson *et al.*<sup>8</sup> using proton beams of 100–200 MeV to study  $(p,n)$  reactions on targets throughout the Periodic Table. The finding<sup>9</sup> that the  $0\hbar\omega$   $1^+$ , Gamow-Teller resonance is the dominant part of the  $(p,n)$  cross section at angles near  $0^\circ$  was followed by the observation of  $\Delta L = 1, \Delta S = 1$  resonances at angles of  $5\text{--}10^\circ$ .

Erell *et al.*,<sup>10</sup> reporting pion charge exchange reactions leading to the emission of neutral pions ( $\pi^\pm, \pi^0$ ), have observed both the isovector monopole resonance and the isovector dipole resonance for the targets  $^{40}\text{Ca}$ ,  $^{60}\text{Ni}$ ,  $^{90}\text{Zr}$ ,  $^{120}\text{Sn}$ , and  $^{208}\text{Pb}$ . These measurements gave

the first observation of the isovector monopole and the zero spin of the pion ensured that the observed resonances were non-spin-flip in nature.

Love and Franey<sup>11</sup> have derived a local nucleon-nucleon effective interaction based on current phenomenological nucleon-nucleon scattering amplitudes, and, using it with the distorted-wave impulse approximation, have applied it to the description of nucleon-nucleus scattering, and, to a lesser extent, to charge-exchange interactions, between 100 and 1000 MeV. This work has demonstrated that, in the energy range 200–400 MeV, the ratio of spin-flip to non-spin-flip isovector transition strengths,  $|J_{\sigma\tau}/J_\sigma|^2$  is of the order of 10. Experimental measurements<sup>12</sup> indicate that the ratio is even higher than predicted by Love and Franey,<sup>11</sup> peaking at a value of about 12.5. The consequence of these observations is that charge-exchange reactions in the energy region 200–400 MeV, will predominantly populate the isovector spin-flip giant resonances.

The distribution of strength in isovector spin-flip giant resonances was calculated in self-consistent Hartree-Fock plus random phase approximation (RPA) theory by Auerbach and Klein.<sup>13</sup> In the case of nuclei with considerable neutron excess, the energies of the three isospin components  $\Delta\tau_z = 0, \pm 1$  are significantly different, these differences being the result of the competing effects of the Coulomb and symmetry potentials. Furthermore, this neutron excess also produces significant Pauli blocking effects. The effects of the neutron excess in Pauli block-

ing are evident in the results of the calculations as one goes from  $\Delta\tau_z = -1$  to 0 to  $+1$ ; in such a progression the number of configurations available to contribute to the formation of the collective state is reduced, and consequently the strength is decreased and the distributions become simpler. These differences in the three isospin projection cases will lead to different escape and spreading widths, accounting for the very different qualitative appearances of the strength distributions of the predicted giant resonances in the different isospin cases.

Thus, on the basis of these calculations,<sup>13</sup> one expects to find in the  $(n,p)$  reaction giant resonances at lower excitation in the residual nucleus and of less complex structure than in the  $(p,n)$  reaction. This prompted a series of experiments, using the TRIUMF charge-exchange facility<sup>14</sup> whose aim was to study the isovector giant resonances excited in  $(n,p)$  reactions on targets whose mass number was in the range 40–238. The proton spectra measured were to be analyzed, using a multipole decomposition procedure, to display the response function of the different nuclei as a function of energy, for the different multipoles. This paper describes the experimental and analysis methods, as well as the results for a  $^{90}\text{Zr}$  target. The  $^{90}\text{Zr}(n,p)$  spectra at 198 MeV have been presented in less detail in an earlier work<sup>15</sup> on this experiment. Candidates for the spin isovector dipole and spin isovector monopole resonances in  $^{208}\text{Pb}(n,p)$  were reported by Moinester *et al.*<sup>16</sup> in a work on another experiment in this series.

Section II of the paper gives the experimental details, and the data reduction processes are described in Sec. III. The final proton spectra from the  $^{90}\text{Zr}(n,p)^{90}\text{Y}$  reaction may be compared with theory in two different ways. The first is to compare the measured spectra with the “total” spectra calculated by Wambach *et al.*,<sup>17</sup> Klein, Love, and Auerbach,<sup>18</sup> and by Yabe,<sup>19</sup> and these comparisons are presented in Sec. IV. The second comparison with theory depends on the decomposition of the experimental spectra into component parts according to some predetermined prescription. Two such decompositions are reported here and their results are compared. The first involves fitting the data with a minimum number of peaks, including a broad one representing the quasifree nucleon charge-exchange scattering. The differential cross-section shapes for the peaks are then deduced, and, from comparison with calculated angular distributions, the multipolarity (the  $L$  transfer of the charge-exchange reaction) or admixture of multipolarities is determined.

The second decomposition method consists of rebining the spectra into 0.8-MeV bins and fitting the angular distribution of each bin with an incoherent sum of the calculated differential cross sections mentioned above. This analysis mode will be referred to as the multipole decomposition (MD) of the spectra.<sup>20</sup>

These methods both require the calculation of “standard” angular distributions, which is described in Sec. V A. The peak-fitting decomposition of the proton spectra is described in Sec. V B, and the multipole decomposition method in Sec. V C. The comparison of the structure of the various multipole giant resonances, as determined by the above methods, with the spectral calcula-

tions of Auerbach and Klein<sup>13</sup> is made in Sec. VI. Section VII presents the conclusions of the work.

## II. EXPERIMENT

The experiment was carried out at the TRIUMF nucleon charge-exchange facility,<sup>14</sup> the layout of which is shown in Fig. 1. The neutrons were produced when a dispersed proton beam, of energy 200 MeV and average intensity 450 nA, struck a narrow strip  $^7\text{Li}$  target of thickness 220 mg/cm<sup>2</sup> and width 7 mm. The proton beam was dispersed in a vertical plane and the strip target was aligned horizontally so that neutrons produced in the  $^7\text{Li}(p,n)$  reaction originated from a very small region and from protons with an energy spread of 350 keV. The primary proton beam, after traversing the  $^7\text{Li}$  target, was bent through 20° and transported to a well-shielded beam dump. Any events from charged particles originating outside the target box were eliminated by the thin veto-scintillator just upstream of the target box. The neutrons produced by this means had a mean energy of 198 MeV in the peak, but the spectrum also exhibited a long tail going to lower neutron energies which was about 1% of the peak in intensity per MeV. The neutrons struck the secondary target assembly which consisted of five foils of  $^{90}\text{Zr}$  (isotopic purity >99%), each of nominal thickness 250 mg/cm<sup>2</sup>, followed by a CH<sub>2</sub> foil of thickness 47 mg/cm<sup>2</sup>. These targets were centered on the axis of rota-

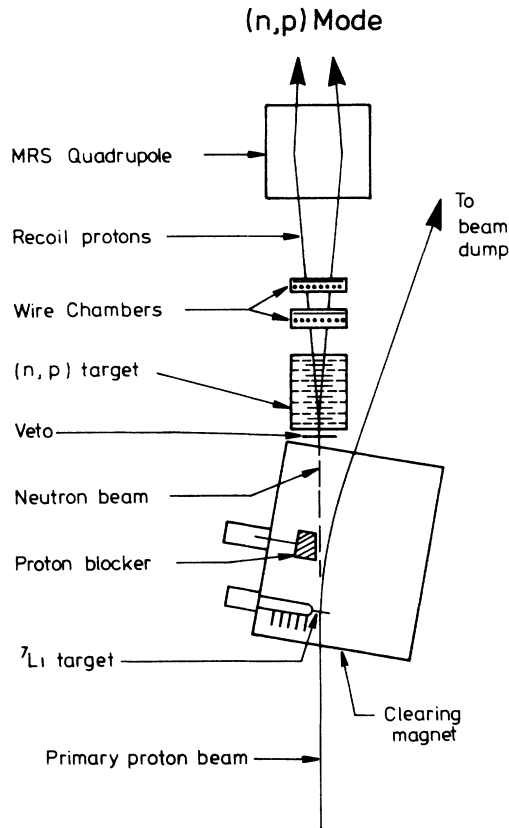


FIG. 1. The layout of the charge-exchange facility at TRIUMF.

tion of the proton spectrometer.

The secondary target foils were separated by multiwire proportional counters (MWPC's). Protons produced by the  $^{90}\text{Zr}(n,p)^{90}\text{Y}$  reaction in a particular target foil would then be expected to produce a signal in all succeeding MWPC's. This feature permits the determination of the layer in which the  $(n,p)$  reaction occurred and hence a correction for the energy loss of the emitted protons in subsequent target layers. A full description of the segmented secondary target system is given in Ref. 21. The protons produced by  $(n,p)$  reactions in the secondary target foils were momentum analyzed by the magnetic medium resolution spectrometer (MRS). This spectrometer has a large momentum acceptance ( $\Delta p/p = 15\%$ ), has an intrinsic resolution of about 100 keV, and has instrumentation which allows good track reconstruction between the target and the focal plane.

"Target empty" runs were taken with no zirconium foils in place; typically these were run for about  $\frac{1}{3}$  of the integrated beam current of the "target in" runs. The main contributions to the "target empty" spectrum came from the following.

- (i) Events in the entrance window of the target box which by-passed the first MWPC and were thus "fed forward" into downstream targets (see later discussion).
- (ii) Events in the Mylar windows of the MWPC's.
- (iii) Events in the  $\text{CH}_2$  target in position six of the tar-

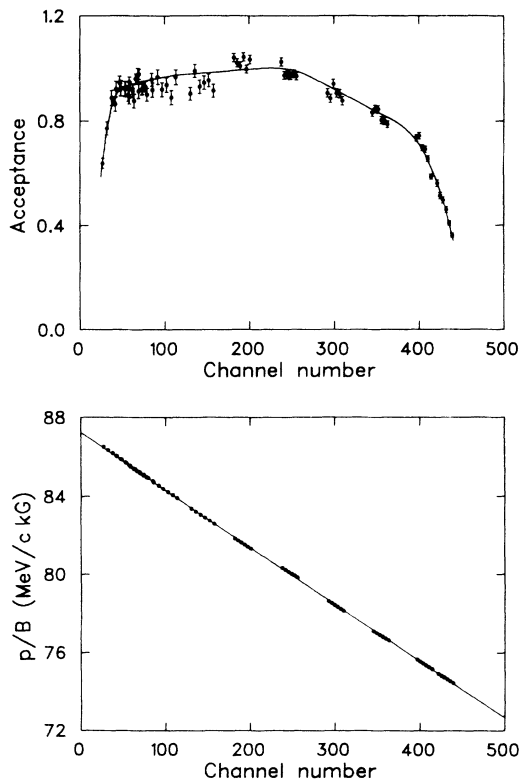


FIG. 2. The upper frame shows the spectrometer momentum acceptance data and the smooth curve used to correct subsequent data. The lower frame is the proton momentum divided by the magnetic field strength versus channel number. This is the calibration curve of the medium resolution spectrometer.

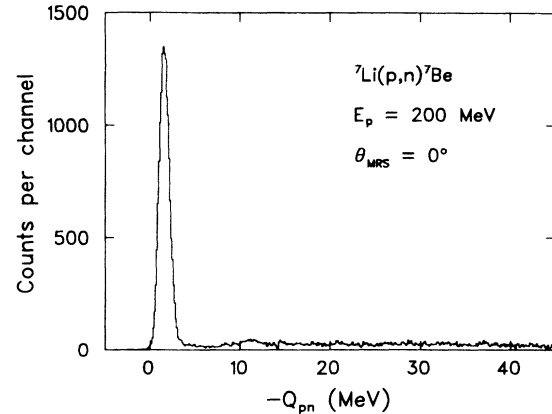


FIG. 3. Neutron spectrum from bombardment of  $220 \text{ mg/cm}^2$   $^7\text{Li}$  by 200-MeV protons.

get stack which occurred in coincidence with a chance random firing of the preceding MWPC and were thus "fed back" into upstream targets (also see later).

At each spectrometer angle, data were also taken with a secondary target stack of six  $\text{CH}_2$  targets. By comparing the relative areas of the  $^1\text{H}(n,p)$  peaks from each target position, the combined effect of the variation of the neutron flux along the target stack and the geometric acceptance of the spectrometer was determined.

At  $\theta_{\text{MRS}} = 0^\circ$ , the spectra from the  $(\text{CH}_2)^6$  stack were recorded for numerous magnetic field settings, chosen so that the resulting positions of the  $^1\text{H}(n,p)$  peak covered the whole of the focal plane. A full size (i.e., not a narrow strip)  $^7\text{Li}$  primary target and achromatic (non-dispersed) beam were used to ensure that the full beam passed through the primary target. The integrated charge from the Faraday cup at the beam dump was used to normalize the peak areas from different runs. Thus, the variation of the areas of the  $^1\text{H}(n,p)$  peaks with focal plane position gave a measure of the momentum acceptance of the spectrometer. The ratio of proton momentum to magnetic field as a function of the focal plane position determined the momentum calibration of the focal plane coordinate. The acceptance curve and the momentum calibration curve of the spectrometer are shown in Fig. 2.

The energy spectrum of the incident neutron beam was determined by measuring the energy of recoil protons from hydrogen in the  $(\text{CH}_2)^6$  target stack. A secondary target stack consisting of five carbon foils followed by a  $\text{CH}_2$  foil for normalization was used to obtain the response of carbon at  $\theta_{\text{MRS}} = 0^\circ$ . After applying the corrections described in the next section, the carbon spectrum was subtracted from the  $\text{CH}_2$  spectrum to give the response of hydrogen alone. This is the neutron spectrum produced in the  $^7\text{Li}(p,n)$  reaction and is shown in Fig. 3. The large peak corresponds to transitions to both the ground state and first excited state at 0.43 MeV in  $^7\text{Be}$ .

### III. DATA REDUCTION

The proton spectra measured by the MRS were collected on magnetic tape in event-by-event mode. Software

corrections to the position on the focal plane were made by ray tracing from the wire chambers at the front end of the spectrometer to the vertical drift chambers near the focal plane. These corrections included both corrections for optical aberrations in the spectrometer and kinematical corrections, and are more fully described in Ref. 14.

For each event, the target layer in which the reaction occurred was identified by considering the pattern of hit wire planes in the  $(n,p)$  target box. It was necessary that two adjacent wires in these planes be struck to register a good hit. This substantially reduced the chance of random hits. The position on the target where the event occurred was determined by tracing back from the front-end chambers to the target plane. In this way, it was possible to eliminate events that originated outside the target dimensions, such as from the target frames.

The true scattering angle for each event was calculated by ray tracing from the primary target (assumed point neutron source) to the event position in the secondary target plane and through to the front-end chambers. Individual target layer spectra were then produced from events in a small angular range. The spectra published in an earlier work on this experiment (Ref. 15) encompassed data from the full  $4.2^\circ$  scattering angle bite of the spectrometer and the mean scattering angle at each spectrometer angle was given. Here, however, events have been grouped into smaller angle bites of  $2.2^\circ$  and though data were taken at only seven spectrometer angles ranging from  $0^\circ$  to  $21^\circ$ , ten spectra were eventually produced with mean laboratory scattering angles between  $1.3^\circ$  and  $22.6^\circ$ .

The inefficiencies of the multiwire proportional counters (wire planes) between the target segments were determined for each run by counting the number of times each wire plane did not fire in an otherwise good event. These inefficiencies, typically 3%, caused a small number of events to be misidentified as originating in the next target downstream rather than the one in which it actually occurred. These are known as feedforwards. By a similar counting method, it was possible to determine the chance of a random firing of one of the wire planes while a real event was being recorded. This was typically 1.5%. These chance events caused a small number of events to be misidentified as originating in the previous target upstream, and are known as feedbacks. The raw spectra were corrected for feedforwards and feedbacks within the stack, and for loss due to inefficiency.

The spectra from the target empty stack were used to estimate the background from  $(n,p)$  events occurring in the counter gas and wire-plane windows. Empirically it is observed that the target empty spectrum contains a larger  $^1\text{H}(n,p)$  peak than can be accounted for by the content of the counter gas and mylar foils alone. There must be a contribution due to events feeding forward from the vacuum entrance window to targets downstream and from events feeding backwards from the  $\text{CH}_2$  target in position six. The same thickness  $\text{CH}_2$  target was used in both the Zr and target empty stacks and so the feedback component should be the same.

The target empty yield was lowest from target position four and so it was assumed that for this target position, the feedforwards from the entrance window and the feed-

backs from target six were negligible. It was then possible to separate the target empty spectra into an anomalous component due only to feedforwards or feedbacks and a background component from materials in the counter gas and mylar windows. When the Zr foils were in positions one to five, the protons that originated within or upstream of the target stack would have lost energy and would be straggled as they passed through the stack. Therefore, we artificially shifted and broadened<sup>22</sup> the different components of the target empty stack spectra according to where they originated.

The individual target spectra of both the target empty and  $^{90}\text{Zr}$  stacks were corrected for the momentum acceptance of the spectrometer and for the neutron flux and geometric acceptance relative to target position six. The total  $^{90}\text{Zr}$  stack and target empty stack spectra were then made by summing together the spectra from each target after first shifting them to correct for energy loss of the protons. The energy loss was calculated (Ref. 23) for protons passing through half the target in which the reaction occurred and all the following targets including the  $\text{CH}_2$  target in position six. The total target empty spectrum was smoothed and normalized [by the ratio of  $^1\text{H}(n,p)$  peak areas from the  $\text{CH}_2$  targets in position six of the Zr and target empty stacks] before subtracting it from the

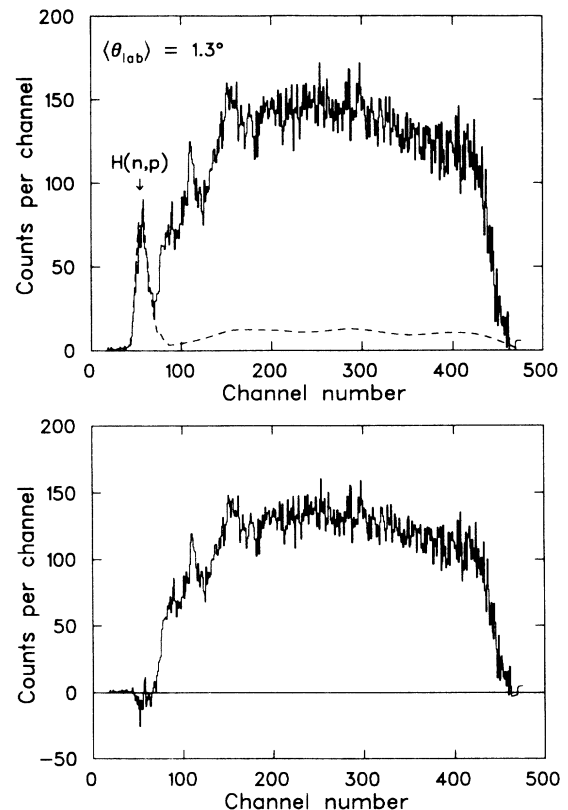


FIG. 4. The upper frame shows the raw spectrum of protons from the  $^{90}\text{Zr}(n,p)^{90}\text{Y}$  reaction with no target empty subtraction (solid) and the summed smoothed target empty spectrum (dashed). The lower frame shows the result of subtracting the empty spectrum from the raw  $^{90}\text{Zr}(n,p)^{90}\text{Y}$  spectrum.

summed Zr spectrum. An excellent check on the corrections to the target empty spectra was how well the  $^1\text{H}(n,p)$  peak, which dominates the target empty spectra, was removed from the summed Zr spectra. This peak is isolated in the spectra taken at mean angles of  $1.3^\circ$  and  $3.3^\circ$  but is kinematically shifted and broadened at larger angles. Figure 4 shows the  $1.3^\circ$  raw proton spectrum on which the summed and smoothed target empty spectrum is plotted. The result of subtracting the target empty spectrum is shown in the lower frame.

After making these corrections, the overall resolution was determined to be 1.3 MeV FWHM. This value was obtained from the width of the hydrogen peak at  $1.3^\circ$ , and is dominated by the contributions of the energy spread of the neutron beam (800 keV) and the energy spread due to energy straggling of protons in both primary and secondary targets (750 keV).

The resultant Zr spectrum at each angle was binned into equal excitation energy increments of 0.4 MeV using the momentum calibration described earlier. The excitation energies are quoted with respect to the  $^{90}\text{Y}$  ground state. The corresponding excitations in  $^{90}\text{Zr}$  occur 13.1 MeV higher, due to the difference in the masses of the  $^{90}\text{Zr}$  and  $^{90}\text{Y}$  ground states (+2.3 MeV), the Coulomb energy difference (+11.6 MeV), and the  $n$ -H mass difference ( $-0.8$  MeV).

As noted in Sec. II, the neutron spectrum produced in the  $^7\text{Li}(p,n)$  reaction by 200-MeV protons is not monoenergetic but consists of a sharp peak followed by a long tail whose intensity per MeV is about 1% of that in the peak. The measured  $^{90}\text{Zr}(n,p)$  spectra must be corrected to remove the effect of this long tail. The  $^7\text{Li}(p,n)$  spectrum was converted to 0.4-MeV bins. All of the counts in the sharp peak were then put into the 0-MeV excitation bin (called the first bin) and the spectrum was normalized such that the value in the first bin was unity. The correction was then made in an iterative process which assumed that the contribution of the tail in the bin corresponding to the ground state of the residual nucleus ( $^{90}\text{Y}$ ) was zero, and that the cross section for the  $^{90}\text{Zr}(n,p)^{90}\text{Y}$  reaction is independent of bombarding energy over a range of 40

MeV, i.e., between 200 and 160 MeV. The tail accompanying events in the first bin of the  $^{90}\text{Zr}(n,p)$  spectrum was subtracted from all higher excitation bins, then the tail accompanying events in the resulting second bin was subtracted from higher bins, and so on.

The unfolding procedure can be written as

$$\begin{aligned} z'_1 &= z_1, \\ z'_i &= z_i - \sum_{j=1}^{i-1} z'_j h_{i+1-j}, \quad i=2,3,\dots, \end{aligned} \quad (1)$$

where  $i$  is the excitation bin number,  $z_i$  is the proton spectrum from the  $^{90}\text{Zr}(n,p)$  reaction,  $z'_i$  is the unfolded proton spectrum, and  $h_i$  is the normalized neutron spectrum from the  $^7\text{Li}(p,n)$  reaction. The effect of this unfolding procedure is shown for the  $3.3^\circ$  spectrum in Fig. 5.

To test the validity of the assumption that the  $^{90}\text{Zr}(n,p)^{90}\text{Y}$  cross section remains constant over 40 MeV, a small linear increase in cross section with decreasing neutron energy was assumed and the unfolding then performed. The increase, which was approximately 0.2% per MeV, was estimated from the magnitudes of calculated cross sections at varying incident energies. The resulting unfolded cross sections were less than 3% different from the unfolded cross sections assuming no energy dependence. In the region of the resonances, the difference was less than 0.5%. Thus, the results discussed henceforth in this paper are those obtained with the assumption of no energy dependence.

The  $^1\text{H}(n,p)$  peak from the  $\text{CH}_2$  target in position six of the Zr stack provided the means of calibrating the cross sections, as data from this target were collected simultaneously with that from the  $^{90}\text{Zr}$  targets. The neutron-proton scattering cross sections in the center-of-mass frame were given by the program SAID (Ref. 24) which uses the Arndt phase shifts. These were converted to  $^1\text{H}(n,p)$  cross sections in the laboratory system and used to normalize the  $^{90}\text{Zr}(n,p)^{90}\text{Y}$  cross sections. The complete set of  $^{90}\text{Zr}(n,p)^{90}\text{Y}$  spectra is shown later in Fig. 10.

#### IV. COMPARISON OF THE DATA WITH THEORETICAL SPECTRUM CALCULATIONS

As noted above, the first comparison is with calculations of the total spectra. Such calculations were first presented by Osterfeld<sup>25</sup> for the related  $(p,n)$  charge-exchange reactions on  $^{40}\text{Ca}$  and  $^{48}\text{Ca}$ . A subsequent paper<sup>26</sup> gave results for the  $^{90}\text{Zr}(p,n)$  reaction. This paper shows that for most of the excitation energy range, the measured  $(p,n)$  spectra can be accounted for by assuming correlated one-particle-one-hole (1p-1h) spin-isospin transitions only, folded with an empirical asymmetric Breit-Wigner shape to simulate the spreading width. In a later calculation of the same reaction, Wambach *et al.*<sup>17</sup> showed that this assumption was essentially correct, because the explicit inclusion of 2p-2h excitations in their reaction calculation made little change to the calculated result.

We observe that the absolute magnitude of the cross

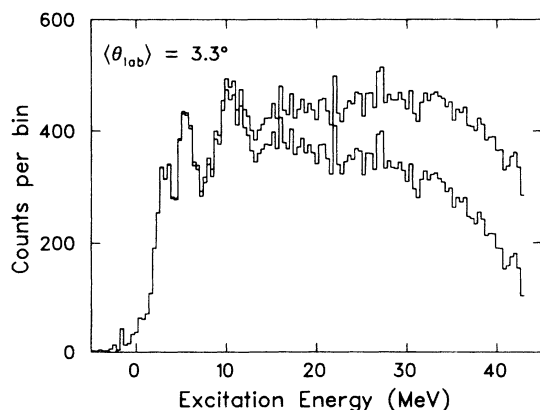


FIG. 5. The  $3.3^\circ$  proton spectrum in 0.4-MeV bins, before and after unfolding the tail of the neutron spectrum. The lower histogram is the unfolded spectrum.

sections presented by Osterfeld *et al.*<sup>26</sup> may be uncertain by as much as 15%. These authors obtain a normalization factor, relating theory to experiment, from the zero degree cross section for the  $^{42}\text{Ca}(p,n)^{42}\text{Sc}(1^+, E_x = 0.61 \text{ MeV})$  reaction. They concluded that a 16% increase in the theoretical cross section was necessary to make it correspond to the experimental result in the  $^{42}\text{Ca}(p,n)$  reaction, and carried that percentage increase over to the  $^{90}\text{Zr}(p,n)$  reaction. They comment further that “the distortion factor  $N_{\sigma\tau}$  could also be responsible for this,” and acknowledge that the extrapolation in  $Z$  noted above “would lead to an uncertainty not larger than 10%.” Furthermore, they point out<sup>26</sup> that at 200 MeV these considerations, and associated parameters, “lead to a 10% larger cross section in  $^{90}\text{Zr}(p,n)$  than those determined from 200 MeV  $(p,p)$  elastic scattering data. Therefore, all our conclusions presented . . . might include such an uncertainty.” It must be concluded, therefore, that while the  $(p,n)$  calculations of Osterfeld *et al.*<sup>26</sup> do fairly well in fitting the spectral shapes, there is significant uncertainty in the absolute cross sections.

Calculations of the  $^{90}\text{Zr}(n,p)^{90}\text{Y}$  reaction spectra have been reported by Klein, Love, and Auerbach,<sup>18</sup> by Yabe,<sup>19</sup> and by Wambach *et al.*<sup>17</sup> These calculations have substantial differences in their bases but have one common feature in their results, which is that they all underestimate the cross section for excitations in  $^{90}\text{Y}$  above about 25 MeV.

Klein, Love, and Auerbach<sup>18</sup> calculated the direct reaction cross section in DWBA. The nuclear structure information was generated using the Skyrme III force to generate the Hartree-Fock single-particle potential, and the transition densities are obtained in the charge-exchange Hartree-Fock random phase approximation framework. Empirical optical-model parameters were used,<sup>27,28</sup> and only correlated 1p-1h states were included. The knock-on exchange term arising from the tensor force was neglected, as was the isovector spin-orbit term. The contributions of both of them were shown to be small. The calculation included only transitions involving states with  $J^\pi \leq 5^+$  ( $L=0-4$ ). The peaks were broadened with a Lorentzian of width 2 MeV. The features of the  $0^\circ$  spectrum, shown in Fig. 6, were dipole peaks at approximately 5- and 14-MeV excitation, and a monopole-quadrupole peak at about 25 MeV. The most obvious shortcoming of this calculation is its inability to predict enough cross section above 30-MeV excitation.

Wambach *et al.*,<sup>17</sup> on the other hand, included 1p-1h and 2p-2h configurations in the random phase approximation, and in a consistent manner included the spreading widths. In a sufficiently heavy nucleus the escape widths are expected to be smaller, and hence were neglected. The reaction calculation was essentially a plane-wave impulse approximation calculation, with the distortion of the optical-model waves approximated by a multiplying factor, a consequence of assuming the distortion function to be local in momentum space. This calculation gives dipole peaks at approximately 3-, 5-, and 11-MeV excitation, with quadrupole peaks of significant strength at 12- and 20-MeV excitation. At  $8^\circ$  and  $10^\circ$ , the calculated energy integrated cross sections (0–50 MeV)

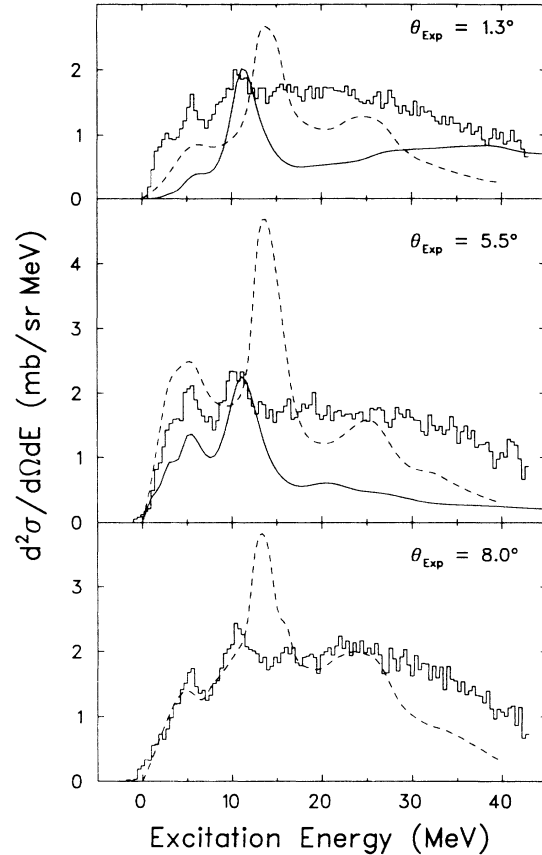


FIG. 6. The experimental spectra at mean angles of  $1.3^\circ$ ,  $5.5^\circ$ , and  $8.0^\circ$  are compared with the calculations of Klein, Love, and Auerbach (Ref. 18) made at  $0^\circ$ ,  $5^\circ$ , and  $8^\circ$  (dashed lines) and those of Wambach *et al.* (Ref. 17) at  $0^\circ$  and  $6^\circ$  (solid lines).

for the dipole and quadrupole contributions are comparable. As with the Klein, Love, and Auerbach calculation,<sup>18</sup> this calculation fails to give enough cross section at high excitations. The results of Wambach’s calculations are also shown in Fig. 6.

The third calculation, which suffers from the same deficiency as the other two, is that of Yabe.<sup>19</sup> This calculation generated the wave functions for the excited states from microscopic RPA calculations, and included configurations up to  $4\hbar\omega$  in energy. All states with  $J^\pi \leq 3^+$  were included. For all the discrete RPA states the differential cross sections were calculated, and from these, continuous spectra by folding them into an asymmetric Breit-Wigner resonance shape. The widths, which varied with excitation, took values from 1 to 15 MeV and were derived from the empirical nucleon-nucleus optical parameters of Rapaport *et al.*<sup>29</sup> The spectra, calculated for proton emission angles of  $0^\circ$ ,  $5^\circ$ , and  $8^\circ$ , showed essentially no structure. A second calculation, using width values of half the magnitude taken previously, gave spectra exhibiting more structure; in particular, there was a substantial peak at an excitation energy of 10 MeV ( $Q$  value of  $-11.5$  MeV), which was stated to be a collective  $2^-$  state. That it is a dipole peak is in agreement with experiment, but this experiment does not confirm that it is a

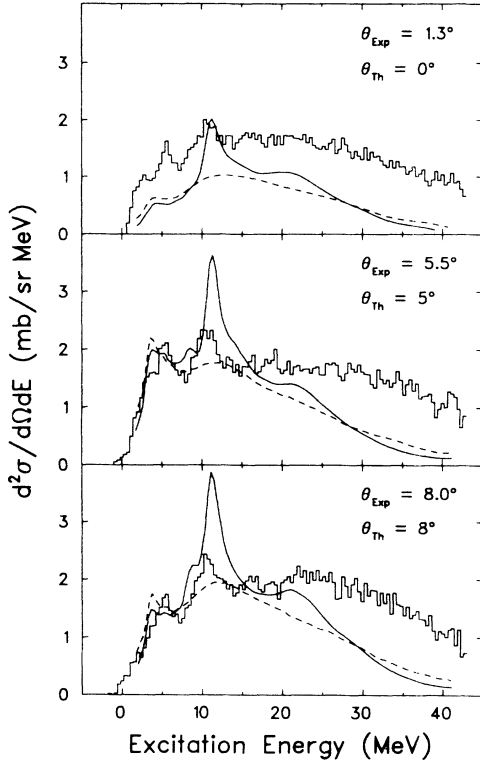


FIG. 7. The experimental spectra at mean angles of 1.3°, 5.5°, and 8.0° are compared with the calculations of Yabe (Ref. 19) at 0°, 5°, and 8°. The dashed lines show the results, with the widths derived from the imaginary part of the empirical optical potential (see text). The solid lines show the results obtained by using smaller widths than those of the dashed lines.

$2^-$  state (see the next section). In this respect, Yabe's calculation disagrees with the structure calculation of Auerbach and Klein,<sup>13</sup> which gives the dipole  $J^\pi$ 's, in order of increasing excitation, as  $2^-$ ,  $1^-$ , and  $0^-$ . Yabe notes<sup>19</sup> that the shapes of the cross sections given by his calculation are similar to that given by Klein, Love, and Auerbach, but that the cross-section magnitudes are a little smaller ( $\approx 15\%$  smaller). This demonstrates that, in all calculations at least, the contributions from the  $L=4,5$  multipoles are small. These were omitted from Yabe's calculation but were included in that of Klein *et al.*<sup>18</sup>

Figure 7 shows that for low excitations ( $< 20$  MeV) the calculations of Yabe<sup>19</sup> give quite a fair representation of the data, the worst agreement being for the case of the 1.3° spectrum. The agreement would be markedly improved by a slight modification of the widths used for the Breit-Wigner shapes. As noted, all calculations fail for the excitation region about 25 MeV.

## V. INTERPRETATION OF THE DATA

### A. Sample angular distributions

Two approaches to the further interpretation of the data were adopted. The first involved fitting a minimum number of some assumed peak shape to the peaks seen in

the data. The second was a multipole decomposition of the data. Both of these methods, which are described shortly, require angular distributions of the differential cross sections for each multipolarity at a number of excitation energies in the residual nucleus. Microscopic particle-hole distorted-wave impulse approximation (PH-DWIA) calculations were performed for many  $J^\pi$  values and excitation energies.

The transition densities were calculated using simple neutron-particle proton-hole wave functions where the strength for each  $J^\pi$  is localized in one coherent state. The amplitude for the different particle-hole components of the wave functions were calculated as the overlap of the appropriate multipole transition operator acting on the assumed closed-shell  $^{90}\text{Zr}$  ground state, and a particular particle-hole configuration,<sup>30</sup> i.e., the excited state  $|X\rangle$  is obtained from the ground state  $|g.s.\rangle$  by

$$|X\rangle = \tilde{O}|g.s.\rangle, \quad (2)$$

where the excitation operator  $\tilde{O}$  is given by

$$\tilde{O} = \sum_{ph} a_p^\dagger a_h \langle ph | \mathcal{M} | g.s. \rangle \quad (3)$$

and  $\mathcal{M}$  is a particular multipole operator, e.g.,  $\mathcal{M} = r^2 Y_2 \sigma \tau$  for a spin isovector quadrupole excitation. The configuration space was restricted to  $\pm 2\hbar\omega$  of the respective neutron and proton Fermi surfaces. The underlying assumption of this method is that all  $p-h$  configurations are degenerate in excitation energy, which is, of course, not true. To test the effect of this assumption, the amplitudes of various  $p-h$  components were varied by 25% (while maintaining a normalized wave function) to simulate the theoretical uncertainties in these wave functions. The resulting angular distributions were found to be insensitive to changes of this magnitude.

The reaction calculations were performed with the code DWBA70 (Ref. 31) which sums the contributions from the different  $p-h$  configurations coherently. The effective interaction used was the  $t$  matrix for free nucleon-nucleon scattering as parametrized by Franey and Love.<sup>11</sup> Some calculations were also performed using the density dependent form of the two-nucleon  $t$  matrix<sup>32</sup> derived from the Paris potential.<sup>33</sup> The differences between calculations for the same transition using the two interactions were negligible over the angular range of interest of the current data. The optical-model potentials (OMP's) used were those of Schwandt *et al.*<sup>28</sup> These are proton-nucleus OMP's and include an energy and target mass dependence. The same parametrization was used for the neutron-nucleus OMP's. Different potentials were tried, such as those of Crawley *et al.*,<sup>27</sup> and the results were found to be insensitive to the choice of a reasonable potential.

Figure 8(a) shows the dipole angular distributions at an excitation energy of 10 MeV for  $J^\pi$  values of  $0^-$ ,  $1^-$ , and  $2^-$ . The small differences in shape between these curves could not be resolved by the data, so an incoherent sum is used to obtain the overall  $L=1$  shape shown in Fig. 8(c). Similarly, the  $L=2, 3$ , and 4 shapes shown in Fig. 8(c) are incoherent sums of the appropriate  $J^\pi$  angular distributions. The  $J^\pi=1^+$  Gamow-Teller (GT) and spin iso-

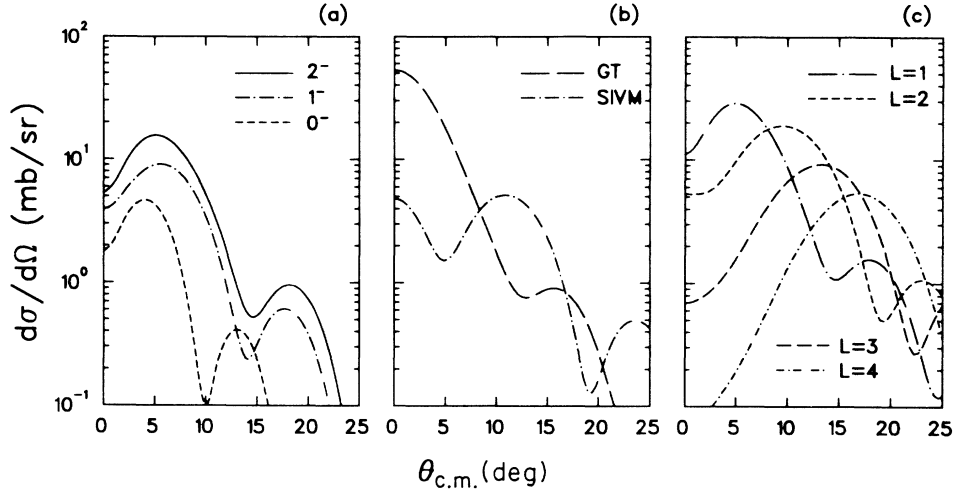


FIG. 8. Results of DWIA calculations of  $^{90}\text{Zr}(n,p)$  at  $E_n = 198$  MeV and an excitation energy of 10 MeV, using 1p-1h amplitudes calculated as described in the text. The  $0^-$ ,  $1^-$ , and  $2^-$  angular distributions are shown in (a). The  $1^+$  GT and SIVM shapes are shown in (b) and the incoherent sums of the appropriate  $J^\pi$  angular distributions for each multipolarity are shown in (c).

vector monopole (SIVM) angular distributions are shown in Fig. 8(b).

### B. Peak fitting

Rather than attempt an overall comparison with theoretical calculations of spectra, as described in Sec. IV, an alternative approach is to fit peaks to the spectral shape at all angles and then to make an interpretation of those peaks. The procedure followed here is similar to that described by Erell *et al.*<sup>10</sup> on the pion charge-exchange reaction which they also used to study isovector giant resonances.

In this case, the dominant and broad peak is ascribed to quasifree scattering at all angles. A symmetric peak shape is assumed, with an exponential cutoff to bring it to zero at a proton energy corresponding to the maximum emitted proton energy less the neutron separation energy of the residual nucleus,  $^{90}\text{Y}$ . Thus, the form of the quasifree fit in terms of the excitation energy  $X$  in  $^{90}\text{Y}$  is

$$\frac{d^2\sigma}{d\Omega dE} = \begin{cases} N \frac{1 - e^{-(X-X_0)/T}}{1 + [(X - X_{QF})/W_L]^2}, & X > X_0, \\ 0, & X < X_0, \end{cases} \quad (4)$$

where  $N$ ,  $X_0$ ,  $T$ ,  $X_{QF}$ , and  $W_L$  are parameters.

In this expression,  $X_0$  is the separation energy of the last neutron in  $^{90}\text{Y}$  (i.e., 6.9 MeV). A quasifree shape calculated with this value of  $X_0$ , and then convoluted with a Gaussian of width 1.3 MeV to simulate the resolution, was negligibly different from a quasifree shape calculated with  $X_0 = 6.6$  MeV. Therefore, in all calculations the value  $X_0 = 6.6$  MeV was used. The quantity  $X_{QF}$  is given by the kinematics of the reaction  $^1\text{H}(n,p)n^*$  where  $m_n^* = m_n + B$ . Here,  $X_{QF}$  is the difference in kinetic energies of the incoming neutron and outgoing proton in this model reaction and  $B$  is a parameter associated with the average binding of struck protons. A value of 12

MeV was used for the parameter  $T$  having been suggested by trial fits to all ten spectra. The quality of the fits is not particularly sensitive to the value of  $T$ . Following Erell *et al.*,<sup>10</sup> we write

$$W_L = W_{L_0} [1 + \alpha(q/k_F)^2], \quad (5)$$

where  $q$  is the momentum transfer at  $X_{QF}$ ,  $k_F$  is the Fermi momentum, and  $W_{L_0}$  and  $\alpha$  are parameters.

The shape of such a fit was checked by comparing it with calculations of the quasifree process by Smith and Wambach,<sup>34</sup> at momentum transfers such that the conditions of validity of the theory are satisfied. The calculations were compared to the empirical fit for  $qR > 1$ , where  $R$  is the nuclear radius and the agreement was good away from the resonance region. The Smith and

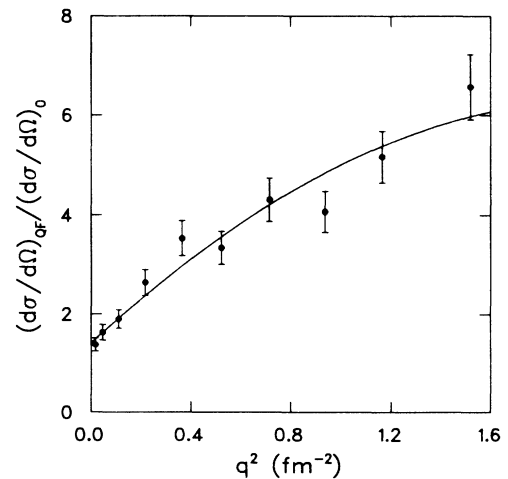


FIG. 9. The ratio of the energy-integrated quasifree cross section to the free  $^1\text{H}(n,p)$  cross section at the  $q^2$  of the peak of the quasifree distribution is plotted against  $q^2$ .

Wambach calculation at angles greater than  $15^\circ$  can be used to give starting values for the parameters  $T$ ,  $B$ ,  $W_{L_0}$ , and  $\alpha$  noted above, since at these angles the peaks in the spectra play a very minor part in determining the spectral shapes. However, it is necessary to use the empirical fit at small excitations as the theory of Smith and Wambach is not valid in that region as it does not take account of the binding energy in  $^{90}\text{Y}$ .

Comparison of an expression of the above form with

individual spectra at small angles led to the conclusion that the minimum number of additional peaks necessary to fit the spectra was four, and this initial analysis also gave starting values for the energies of the peaks (on the  $^{90}\text{Y}$  excitation energy scale), their widths and their peak cross sections at each angle.

Having these sets of starting values, the ten spectra, at mean scattering angles from  $1.3^\circ$  to  $22.3^\circ$ , were all fitted simultaneously for minimum  $\chi^2$ . The parameters that

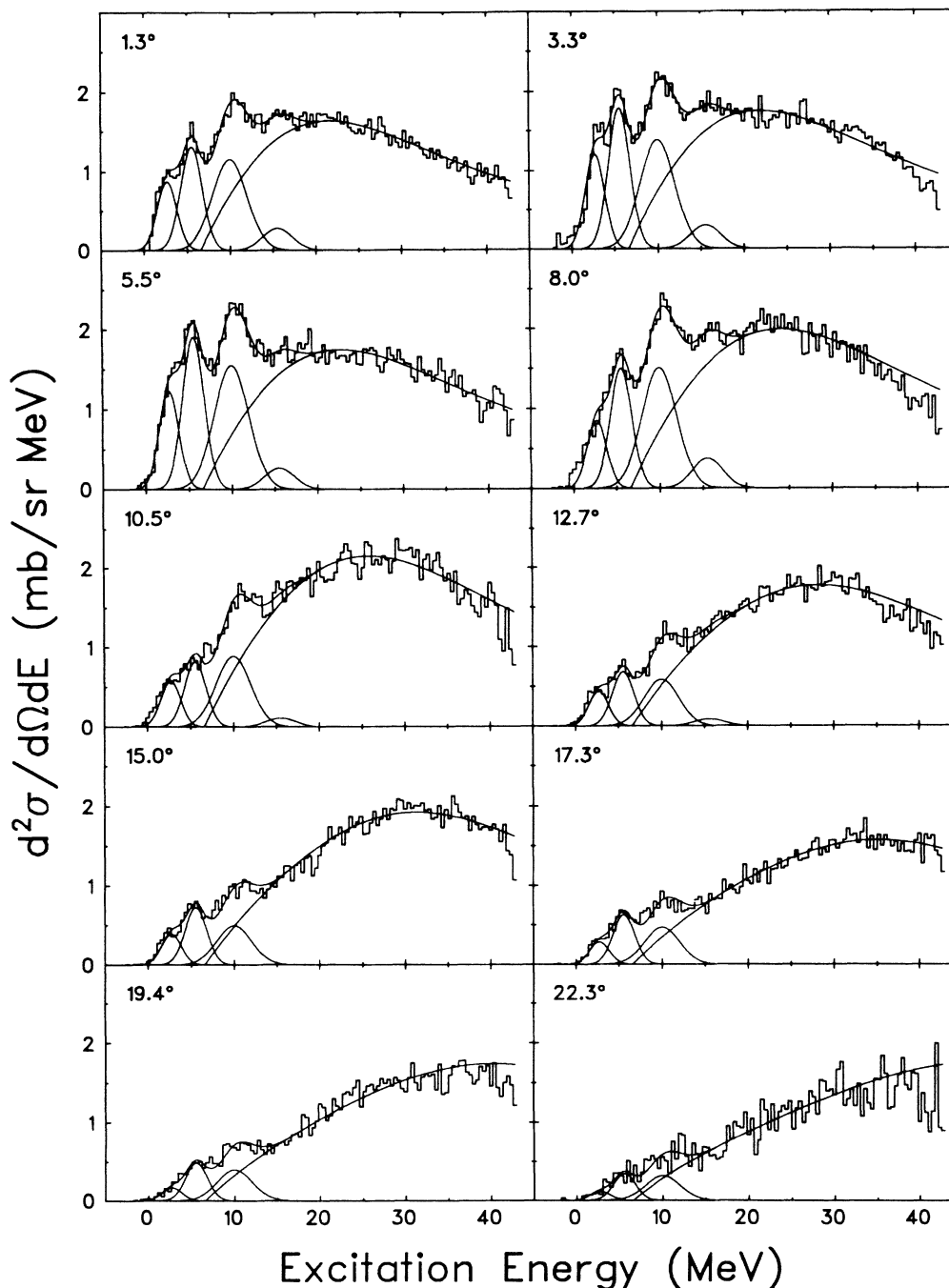


FIG. 10. The fitting of four peaks, plus the quasifree scattering shape, to the ten spectra is shown. Note that all spectra were fitted simultaneously.

were varied in the fit were  $B$ ,  $W_{L_0}$ ,  $\alpha$ , and ten  $N$ 's (one for each angle). It is emphasized that no constraint was placed on the normalization  $N$  of the quasifree peak in any spectrum. This quantity was allowed to vary freely in the fitting. However, at the completion of the fitting, the  $q^2$  dependence of the energy-integrated quasifree cross section was plotted, and was shown to be closely linear as a function of  $q^2$  for small  $q$  (see Fig. 9) as is expected, since a cross section must be an even function of the scattering angle.

The results of this fitting of ten spectra are shown simultaneously in Fig. 10, and the parameters for the quasifree scattering and the four extra peaks are shown in Table I.

Having consistent fits to all the measured spectra, the differential cross sections for the four peaks were plotted, as shown in Figs. 11(a)–11(d). Figures 11(a)–11(c) show differential cross sections whose shapes are qualitatively similar. The differential cross sections for the peaks at excitations 2.7, 5.5, and 10.0 MeV are well fitted by an incoherent sum of Gamow-Teller,  $L = 1$  and 3 angular distributions which were calculated as described in the previous section. In each of these peaks the  $L = 1$  transitions dominate, with a significant component of  $L = 3$  transitions being present. Since the  $L = 1$  spin-flip transitions populate states of  $J^\pi = 0^-, 1^-,$  and  $2^-$ , and  $L = 3$  transitions populate states of  $J^\pi = 2^-, 3^-,$  and  $4^-$ , a component of both the  $L = 1$  and 3 strengths could be due to  $2^-$  states. The cross section for Gamow-Teller transitions will be discussed in the next section.

It is noted that in no case do the fits pass near the  $20.1^\circ$  and  $22.9^\circ$  points. This most probably signals the presence of  $L$  values higher than 3, possibly the presence of high-spin states or an inadequate treatment of the quasifree continuum.

The fourth peak, centered at 15.5 MeV, exhibits a differential cross section which resembles qualitatively

TABLE I. Parameters of the Gaussian peaks and quasifree scattering shape used to fit the spectra shown in Fig. 10.

$E_0$ (MeV)	$\Gamma^a$ (MeV)	Gaussian peaks	
		GT	SIVD
2.7	2.3	1.9	2.9
5.5	2.6	2.4	5.2
10.0	4.6	1.6	7.5
15.5	3.8	b	

Quasifree shape	
$X_0 = 6.6$ MeV	(see text)
$T = 12$ MeV	
$B = 11.9$ MeV	
$W_{L_0} = 22.7$ MeV	
$\alpha/k_F^2 = 0.36$ fm <sup>2</sup>	

<sup>a</sup> These figures represent the natural FWHM. The resolution width of 1.3 MeV has been removed in quadrature.

<sup>b</sup> For possible composition of this peak, see text.

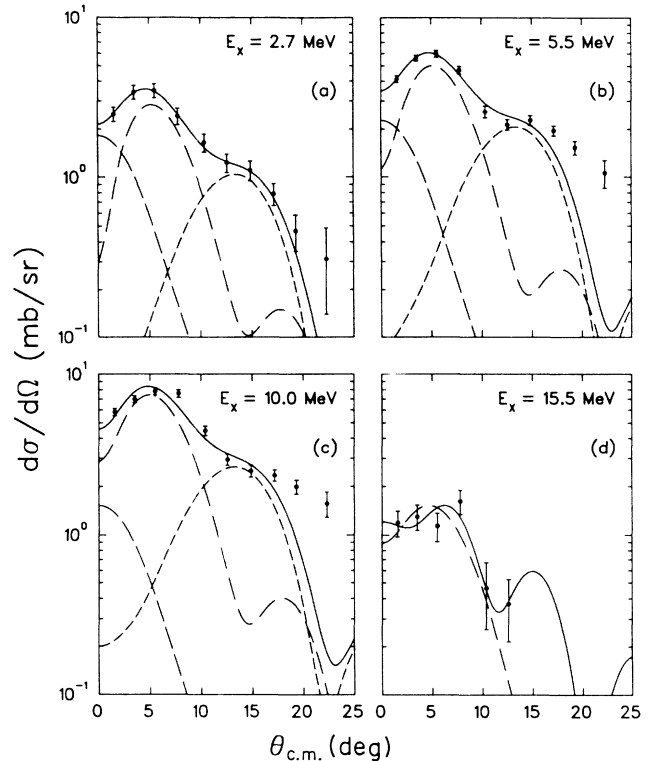


FIG. 11. Differential cross sections for the four peaks are shown, as well as the fits to them from the incoherent sums of sample angular distributions. The line types are as specified on Figs. 8(b) and 8(c). The uncertainties on the data include the overall uncertainty in the normalization of the spectra at each angle and the uncertainties due to fitting the peaks but do not include a systematic uncertainty contribution due to the choice of background. This is expected to increase with angle.

that of the spin isovector monopole angular distribution. However, measured angular distribution for that peak is significantly lower than the calculated SIVM distribution. An attempt was made to fit this angular distribution using a coherent sum of SIVM and spin isovector quadrupole (SIVQ)  $1^+$  transition amplitudes specified as follows:

$$A_{1^+} = \frac{\alpha}{(\alpha^2 + 1)^{1/2}} A_{\text{SIVM}} + \frac{1}{(\alpha^2 + 1)^{1/2}} A_{\text{SIVQ}} \quad (6)$$

The fit shown in Fig. 11(d) was obtained with a value of  $\alpha = -0.7$ . However, as shown by the dashed curve in Fig. 11(d), an  $L = 1$  angular distribution fits the experimental data almost as well. This situation does not encourage any definite conclusion in the case of this peak.

Perhaps the most surprising aspect of this spectral decomposition is the dominance, in magnitude, of the quasifree charge-exchange scattering. This is in direct contrast to the  $(p, n)$  reaction spectra,<sup>6,7</sup> where the dominant feature is undoubtedly the Gamow-Teller resonance. Indeed, if one removes the GT resonance from consideration, the  $(p, n)$  and  $(n, p)$  cross sections for a given target are similar in magnitude.

### C. Multipole decomposition

The second method used for identifying and extracting the giant resonance strengths was a multipole decomposition of the experimental spectra. The basic assumption of this method is that any interference between the various multipole transitions making up the spectra is small.

The measured spectra were put into excitation energy bins of width  $\Delta E = 0.8$  MeV. This binwidth is convenient as it is close to half the experimental resolution, and gave excitation energy bins centered at close to the observed local maxima in the low angle spectra.

For each excitation energy bin, the angular distribution of the differential cross section was extracted. Using the assumption that the multipoles do not interfere with each other, this differential cross section can be written as

$$\left( \frac{d\sigma}{d\Omega} \right)_{\text{expt}} = \sum_L a_L \left( \frac{d\sigma}{d\Omega} \right)_L, \quad (7)$$

where  $a_L$  are the relative strengths of each of the multipoles and are functions of excitation energy only,  $(d\sigma/d\Omega)_L$  are the angular distributions for each of the multipoles, normalized to unity at the peak value, and  $L$  is the orbital angular momentum associated with each of the giant resonances.

The problem then was to find the  $a_L$  values for each excitation increment given a set of angular distributions  $(d\sigma/d\Omega)_L$ . A semiclassical calculation indicates that  $L$  values up to a maximum of approximately 7 are possible

for the angular range covered by this experiment. Also, as indicated before, the transitions are predominantly spin flip and so, except for  $L=0$ , there are three possible  $J^\pi$  values for each  $L$  value. There are clearly too many degrees of freedom for the resolution and angular range of the data. For this analysis it was sufficient to consider a maximum of  $L=4$  only.

The DWIA calculations indicate (as do the more detailed RPA-DWIA calculations of Klein, Love, and Auerbach<sup>18</sup> that the theoretical angular distribution shapes are somewhat different for the different  $J^\pi$ 's and have different strengths. The differences though, are small, and it is sufficient to group the  $J^\pi$ 's according to orbital angular momentum transfer  $L$ . Thus, for  $L \neq 0$ , the generalized theoretical shape  $(d\sigma/d\Omega)_L$  is given by the sum of the DWIA calculations appropriate for that multipolarity. Symbolically, this grouping is

$$L=1 \supset (J^\pi = 0^-, 1^-, 2^-), \quad L=2 \supset (J^\pi = 1^+, 2^+, 3^+),$$

$$L=3 \supset (J^\pi = 2^-, 3^-, 4^-), \quad L=4 \supset (J^\pi = 3^+, 4^+, 5^+).$$

Other groupings are possible and these will be discussed later with reference to the stability of the results.

There are two other possibilities. These are both  $J^\pi = 1^+$  and are the  $0\hbar\omega$  Gamow-Teller and the  $2\hbar\omega$  spin isovector monopole transitions. The angular distributions of both of these peak at  $0^\circ$  [see Fig. 8(b)] and even though the shapes are somewhat different at larger angles, a multipole decomposition of a limited data set can-

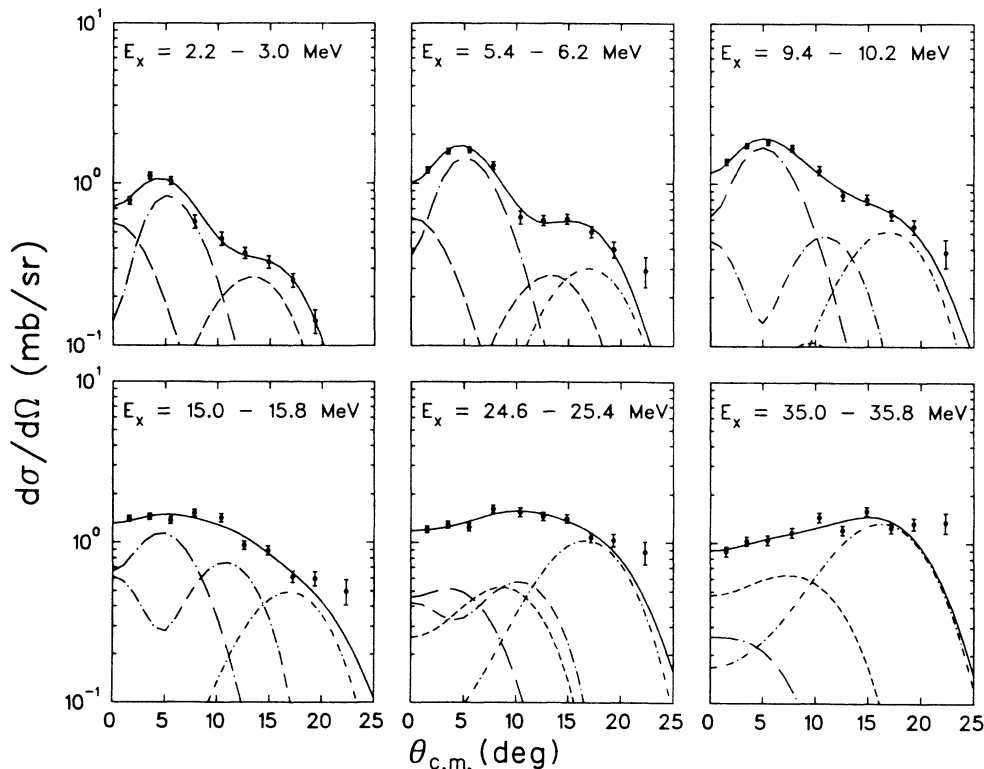


FIG. 12. Sample differential cross sections for the protons in six different excitation energy bins. These are chosen to be typical of the angular distributions observed in this experiment. The line types are as specified on Fig. 8.

not distinguish between SIVM and the sum of GT and spin isovector quadrupole angular distributions. Therefore, to avoid misassigning SIVM strength at higher excitations as GT strength, it is necessary to choose an excitation energy at which to separate either the GT and SIVM or the GT and SIVQ shapes. Below this energy, either the SIVM or SIVQ was set to zero and above it the GT was set to zero in the decomposition.

We are guided, first, by theoretical calculations in making the choice of an appropriate excitation energy at which to split the  $1^+$  transitions. Bloom *et al.*<sup>35</sup> have calculated the Gamow-Teller strength function for the  $^{90}\text{Zr}(n,p)^{90}\text{Y}$  reaction at 200 MeV using two extreme models. The strength function from both models goes to zero for excitations greater than 8 MeV. Auerbach and Klein have made calculations<sup>13</sup> which predict no SIVM strength below 7.8 MeV. Our first choice was to separate the GT and SIVM at 7.8 MeV as this is one of the boundaries between the excitation bins used in the decomposition.

A further test was made in an attempt to clarify the separation of Gamow-Teller and SIVM strength. In this case the SIVQ strength was put identically to zero, and both Gamow-Teller and SIVM shapes were used in the multipole decomposition. The result of this test was that the GT strength went smoothly to zero above 11-MeV

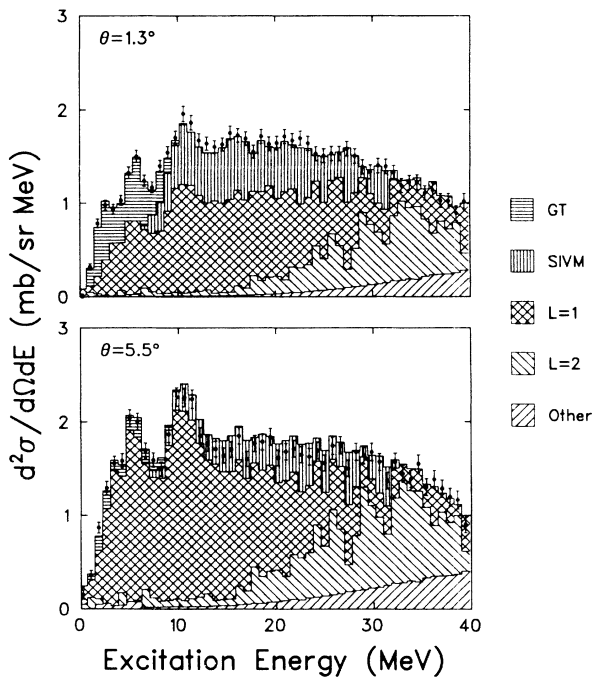


FIG. 13. Multipole decomposition of the  $^{90}\text{Zr}(n,p)^{90}\text{Y}$  spectra at angles close to the maximum of the GT and dipole angular distributions. The contributions of each component to the total reconstructed spectra are indicated by the shaded regions. A key to the types of shading is given. The uncertainties on the data included the statistical uncertainties for each bin and the uncertainty in the overall normalization of each spectrum. The normalizations of the spectra are independent and so are important in the decomposition which depends upon angular distributions.

excitation and the SIVM strength rose from almost zero below 5 MeV. Further, what was taken to be SIVQ in previous decompositions was, in this test, taken up into the SIVM strength.

As a consequence of this test, the final conditions for the decomposition were that the GT strength was constrained to go smoothly to zero for excitations from 7.8 to 11 MeV and the SIVM strength was constrained to rise smoothly from zero for excitations from 4.6 to 7 MeV. Figure 12 shows the experimental differential cross sections for several excitation increments. Also shown are the various multipole components which were added incoherently to give the overall fit. The fitted strengths can be used to “reconstruct” the spectra by multiplying them by the appropriate DWBA cross section at each angle. This is shown in Fig. 13 for the lowest angle, which is near the maxima of the GT and SIVM angular distributions, and at an angle close the maximum of the dipole angular distribution. The distributions in excitation energy of the peak values  $a_L$  of the components are shown in Fig. 14(a). A decomposition of the nonresonant (quasi-free) components of the spectra was also made. The resulting strength functions were subtracted from those of the total spectra. The differences are shown in Fig. 14(b).

## VI. DISCUSSION

The  $^{90}\text{Zr}(n,p)^{90}\text{Y}$  reaction has been studied for a neutron energy of 198 MeV, by detection of the emitted protons. The spectra of these protons display spin-flip isovector giant resonances.

The treatment of the data has been described in detail, and three different methods for comparison of the results with theory have been used. They are the following.

(i) The comparison of measured proton spectra with calculations of the total proton spectra.

(ii) The fitting of Gaussian peaks, plus a quasifree scattering shape to the spectra, followed by a deduction of the multipolarities present in each of the peaks from comparison with sample calculated angular distributions.

(iii) A multipole decomposition of the proton spectra, using the sample calculated angular distributions.

The latter two methods give consistent results, indicating a small amount of Gamow-Teller strength at low excitations in  $^{90}\text{Y}$ , some spin isovector monopole strength at higher excitations, substantial spin isovector dipole strength, and possibly a small amount of spin isovector quadrupole strength. It must be noted that the angular distribution shapes which were calculated indicated that it would be virtually impossible to distinguish between the spin isovector monopole contribution and the sum of Gamow-Teller and spin isovector quadrupole angular distributions. The discussion of the strengths of the multipoles is now dealt with separately.

### A. Gamow-Teller strength

The total Gamow-Teller strength was calculated from both the peak-fitting results and from the multipole decomposition results using the relation

$$\frac{d\sigma}{d\Omega}(0^\circ)/S_{\beta^+} = 4.2 \text{ mb/sr} . \quad (8)$$

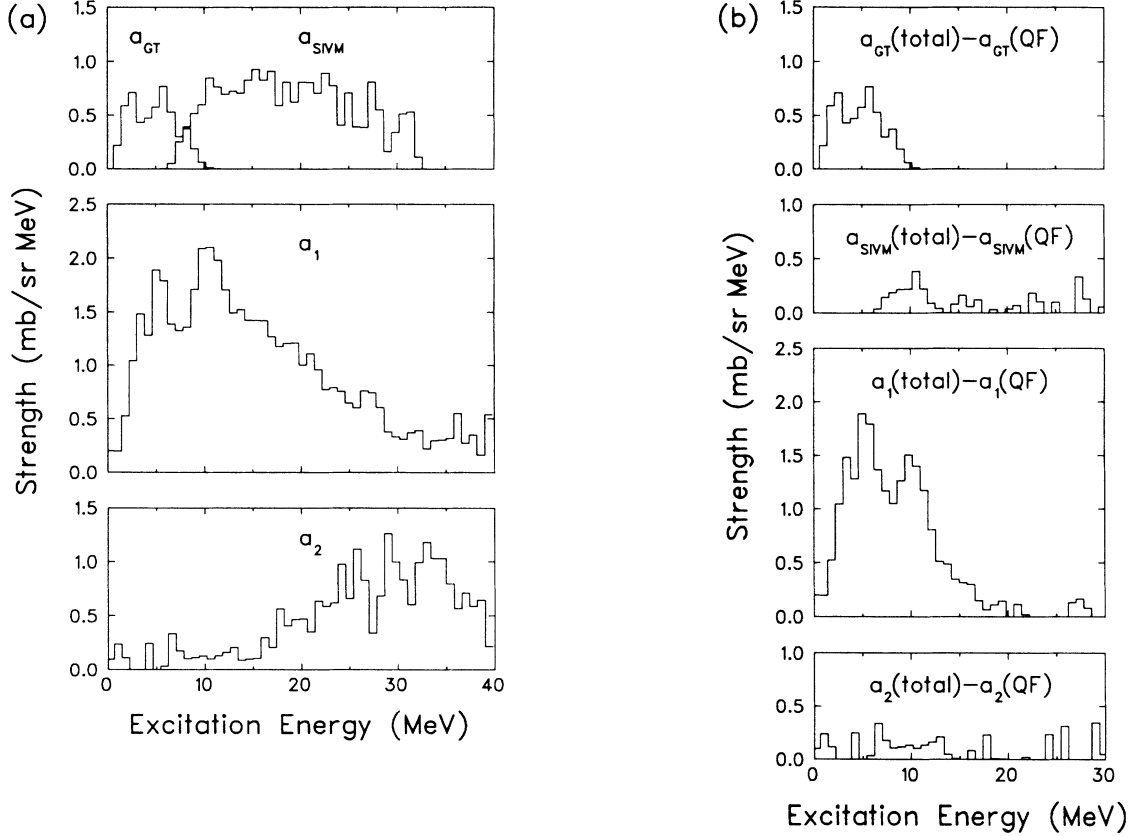


FIG. 14. The strength functions for Gamow-Teller and SIVM transitions, and spin dipole and spin quadrupole transitions, as determined by the multipole decomposition procedure described in the text. The results for the decomposition of the total spectra are shown in (a), and for the total spectra minus the quasifree contributions in (b).

The value of 4.2 mb/sr was obtained from a calculation<sup>36</sup> of the cross section per unit GT strength for the  $^{90}\text{Zr}(p,n)$  reaction. Taddeucci *et al.*<sup>37</sup> also give a value near 4 mb/sr for the  $^{90}\text{Zr}(p,n)$  reaction at 200 MeV. These calculations are based on the relation<sup>38</sup>

$$\frac{d\sigma}{d\Omega}(q, X) = KN_{\sigma\tau}^D |J_{\sigma\tau}|^2 B(\text{GT}), \quad (9)$$

where  $K$  is a kinematic factor,  $N_{\sigma\tau}^D$  is the distortion factor defined by the ratio of plane-wave and distorted-wave cross sections,  $J_{\sigma\tau}$  is the volume integral of the spin-flip isospin-flip part of the nucleon-nucleon interaction, and  $B(\text{GT})$  is the GT beta decay transition strength.

All the nuclear structure effects, including Pauli blocking, are contained in  $B(\text{GT})$  and the total strength is given by

$$S_{\beta} = \sum B(\text{GT}), \quad (10)$$

where the sum is over all final states. Thus, apart from small differences in distortion and kinematics, the proportionality factor (4.2 mb/sr) should be the same for the  $(p,n)$  and the  $(n,p)$  reaction.

The best estimate of  $S_{\beta^+}$  comes from the multipole decomposition technique using the assumption described earlier that the distribution goes smoothly to zero at 11

MeV. The confidence limits for  $S_{\beta^+}$  are difficult to estimate, because they depend as much on the accuracy of the sample angular distributions for each  $L$  value (in particular, the low angle behavior of the  $L=1$  distribution which is due to the distortion of the incident and outgoing waves in the DWIA calculation), as on the statistics of the experimental yields or the particular details of the peak-fitting or multipole decomposition method of analysis. Our best estimate under the above assumption would have the result for Gamow-Teller strength stated as  $1.0 \pm 0.3$  units. The uncertainty in this and the following estimates does not include any uncertainty in the ratio 4.2 mb/sr given above.

In an attempt to obtain an upper limit of the Gamow-Teller strength, decompositions were made under different assumptions. The result from the peak fitting assumes no monopole strength below about 10 MeV and allows GT strength up to a little above 15 MeV. A non-resonant (quasifree) background was included in the fitting and no strength was assigned to it. The value of  $S_{\beta^+}$  from this method is 1.4 units.

A decomposition was done in which no monopole strength was allowed anywhere and no quasifree background was subtracted. As expected, the sum of Gamow-Teller and quadrupole angular distributions

played the role of the monopole, and the Gamow-Teller strength did not fall until about 30 MeV in excitation. The total GT strength up to 20 MeV (see later) from this decomposition is 3.3 units.

These estimates of Gamow-Teller strength are to be compared with the strength calculated by Bloom *et al.*<sup>35</sup> of 1.6 (their model *A*) and that of 1.2 calculated by Kuz'min and Soloviev.<sup>39</sup> In both cases the agreement is satisfactory. As noted above, the distribution calculated by Bloom *et al.*<sup>35</sup> is limited to the excitation region below 8 MeV in <sup>90</sup>Y. The distribution calculated by Kuz'min and Soloviev,<sup>39</sup> on the other hand, extends from the ground state up to an excitation of about 18 MeV.

A value of  $0.12 \pm 0.18$  units of GT strength was obtained from the <sup>90</sup>Zr(*n,p*) reaction at 65 MeV (Ref. 40) and is also be compared to the estimates of this work. However, this value must be very uncertain because of the unknown normalization of the preequilibrium component and the large effect of distortion at 65 MeV.

### B. Spin isovector dipole strength

The peak-fitting analysis indicated that the peaks centered at 2.7-, 5.5-, and 10.0-MeV excitation in <sup>90</sup>Y were dominated by spin isovector dipole transitions and this is strongly supported by the multipole decomposition. These excitation energies correspond to excitations in <sup>90</sup>Zr of 15.8, 18.6, and 23.1 MeV, respectively. As indicated in Sec. IV (above) and Figs. 6 and 7, the calculations of total spectra would appear to show that the calculated and measured SIVD strengths agree within a factor of 2. However, the SIVD strength found experimentally is more widely spread in energy than the very narrow distribution indicated in the paper of Auerbach and Klein.<sup>13(b)</sup>

Auerbach, Klein, and Love<sup>36</sup> have calculated the integrated (*n,p*) cross sections for transitions which populate the  $J^\pi = 0^-, 1^-,$  and  $2^-$  states which can be populated by  $L = 1$  transitions. They give 29 mb/sr for this value which is to be compared with values of 38 mb/sr from the multipole decomposition to 40-MeV excitation or 16 mb/sr from the peak fitting with quasifree contribution subtracted.

### C. Spin isovector monopole and quadrupole strength

As shown in Fig. 14(a), the best estimate of the strength of SIVM transitions is spread more or less uniformly between about 10 and 25 MeV. This is not in contradiction with the calculations of Auerbach and Klein,<sup>13</sup> particularly when a resolution function of width 1.3 MeV is used to smooth the calculation. The matter of SIVM strength will be considered together with the SIVQ strength.

Auerbach and Klein<sup>13(b)</sup> have calculated the total SIVM and SIVQ strengths and find their ratio to be  $\frac{1}{2}$ . To compare this number with an experimental ratio, this number must be modified by a reaction calculation using the DWBA. Such a calculation finds the SIVM peak cross section to be approximately half the SIVQ peak cross section for a residual excitation of 20 MeV. In that

TABLE II. The total GT strength and ratios of SIVM to SIVQ strengths resulting from possible misassignment fractions (see text). The discrepancy of the SIVM-SIVQ ratio to that predicted by Auerbach and Klein [Ref. 13(b)] is also given.

Misassignment fraction <sup>a</sup>	GT strength (consequent)	SIVM strength / SIVQ strength (to 40 MeV)	Discrepancy from theory (factor)
0	1.0	0.86	3.4
0.5	2.1	0.48	1.9
0.75	2.7	0.34	1.4

<sup>a</sup> The Auerbach and Klein calculation [Ref. 13(b)] indicates significant SIVM strength below 20-MeV excitation.

situation one would expect the ratio of cross sections to be about  $\frac{1}{4}$ . Because of the inability to separate the SIVM contribution from the (GT plus SIVQ) contribution, any argument based on the experimental results must involve all three.

The Gamow-Teller contribution is expected to be confined to excitation energies below 20 MeV since it must arise from ground-state correlations in <sup>90</sup>Zr. Certainly the two calculations of the GT strength distribution as a function of excitation energy<sup>35,39</sup> show it going to zero before that excitation. Table II shows the consequence of assuming three different fractions of the SIVM strength below 20 MeV to have been misassigned, i.e., assigned to SIVM instead of to GT plus SIVQ. It is clear that the data are not inconsistent with the prediction of the SIVM-to-SIVQ ratio by Auerbach and Klein,<sup>13(b)</sup> nor are they inconsistent with the GT predictions of Bloom *et al.*<sup>35</sup> or Kuz'min and Soloviev.<sup>39</sup> However, these two statements are not mutually exclusive inasmuch as the data are not consistent with both the SIVM-to-SIVQ ratio prediction and the GT prediction simultaneously.

However, a word of caution must be given regarding the taking of this result as more than just the indication of a possibility. Since the highest  $L$  value considered in the multipole decomposition is 4, the result for  $L = 2$  considered above must be marginal, and those for  $L = 3, 4$  not to be believed.

## VII. CONCLUSIONS

It is worth pointing out that the  $L = 0$  and 1 conclusions are quite stable under variations of the conditions under which the multipole decompositions were made. This involved performing the decompositions with three, four, or five degrees of freedom. The number of shapes used in the decomposition was limited by combining, for example, the  $L = 3$  and 4 shapes into a composite shape.

A complementary experiment, in which the reaction <sup>90</sup>Zr(<sup>7</sup>Li, <sup>7</sup>Be)<sup>90</sup>Y was studied, has been reported by Gareev *et al.*<sup>41</sup> That experiment concludes that, in the excitation region up to 3 MeV, the transitions with  $L = 1$  and 3 are dominant, between 3 and 8 MeV no single multipolarity dominates over all others, and for excitation energies above 8 MeV,  $L = 4$  and 6 are dominant. How-

ever, the relatively featureless angular distributions found in that experiment must make the drawing of conclusions difficult. Furthermore, the interpretation of the results appears to depend critically on the calculated particle-hole spectrum of  $^{90}\text{Y}$  which was also reported in the above-mentioned work. Nevertheless, the conclusions do, in some respects, resemble those of this work, in that the dominance of  $L = 1$  transitions at low excitations is confirmed although the heavy-ion experiment does find more  $L = 3$  strength than the present analysis indicates. A four-peak decomposition of the ( $^7\text{Li}, ^7\text{Be}$ ) spectra gives peaks at excitations of 1.7, 4.6, 8.4, and 14.8 MeV with widths of 2.2, 3.0, 7.0, and 13.9 MeV, respectively. These values are to be compared with 2.7-, 5.5-, 10.0-, and 15.5-MeV excitation energies, and widths of 2.3, 2.6, 4.6, and 3.8 MeV reported here. No reason can be given for this discrepancy, which averages about 1 MeV in the excitation energies.

Brady *et al.*<sup>40</sup> have measured the  $^{90}\text{Zr}(n,p)^{90}\text{Y}$  at 65 MeV, and report structure at low excitations which appears to be dominated by spin dipole strength at excitations of 1.8, 5.6, and 10.4 MeV. These values agree, within the combined uncertainties, with those obtained in this work. The confidence level of the quantitative results quoted must, however, have been affected by the dominance of the preequilibrium continuum background that was subtracted before analysis of the spectra.

The conclusions of this investigation may then be stated as follows.

(i) The best estimate of the Gamow-Teller strength ob-

served in the  $^{90}\text{Zr}(n,p)^{90}\text{Y}$  reaction at 200 MeV is close to 1 unit where the units are those of the Ikeda sum rule

$$S_{\beta^-} - S_{\beta^+} = 3(N - Z) .$$

(ii) Taking the above result for GT strength as close to true, the ratio of spin isovector monopole to spin isovector quadrupole strength is indicated to be greater than given in the structure calculations.<sup>(13b)</sup> However, the data are consistent with the SIVM-to-SIVQ ratio calculation but in this case the consequent GT strength is close to 3 units.

(iii) The spin isovector dipole strength observed is approximately that given by theory,<sup>17-19</sup> though rather more spread out in energy.

(iv) The high excitation continuum region of the spectra is not well predicted by theory. In particular, all available calculations underestimate the strength at high excitations.

#### ACKNOWLEDGMENTS

The authors are grateful to Dr. W. G. Love, Dr. S. D. Bloom, Dr. R. Smith, Dr. J. Wambach, Dr. N. Auerbach, and Dr. A. Klein for useful discussions and permission to show the results of their calculations. The authors are also grateful to Dr. A. Trudel for her help with the calculation of the transition densities used in the DWIA calculations. This research was supported in part by the National Sciences and Engineering Research Council of Canada and by the Australian Research Grants Scheme.

<sup>1</sup>G. C. Baldwin and G. S. Klaiber, *Phys. Rev.* **73**, 1156 (1948).

<sup>2</sup>M. Goldhaber and E. Teller, *Phys. Rev.* **74**, 1046 (1948).

<sup>3</sup>M. Lewis and F. E. Bertrand, *Nucl. Phys.* **A196**, 337 (1972).

<sup>4</sup>R. Pitthan and Th. Walcher, *Phys. Lett.* **36B**, 563 (1971).

<sup>5</sup>S. Fukuda and Y. Torizuka, *Phys. Rev. Lett.* **29**, 109 (1972).

<sup>6</sup>R. R. Doering, A. Galonsky, D. M. Patterson, and G. F. Bertsch, *Phys. Rev. Lett.* **35**, 1691 (1975).

<sup>7</sup>D. E. Bainum, J. Rapaport, C. D. Goodman, D. J. Horen, C. C. Foster, M. B. Greenfield, and C. A. Goulding, *Phys. Rev. Lett.* **44**, 1751 (1980).

<sup>8</sup>B. D. Anderson, T. Chittrakarn, A. R. Baldwin, C. Lebo, R. Madey, P. C. Tandy, J. W. Watson, B. A. Brown, and C. C. Foster, *Phys. Rev. C* **31**, 1161 (1985).

<sup>9</sup>C. Gaarde, *Nucl. Phys.* **A396**, 127 (1983); C. D. Goodman, *Prog. Part. Nucl. Phys.* **11**, 475 (1984).

<sup>10</sup>A. Erell, J. Alster, J. Lichtenstadt, M. A. Moinester, J. D. Bowman, M. D. Cooper, F. Irom, H. S. Matis, E. Piasezky, and U. Sennhauser, *Phys. Rev. C* **34**, 1822 (1986).

<sup>11</sup>W. G. Love and M. A. Franey, *Phys. Rev. C* **24**, 1073 (1981); M. A. Franey and W. G. Love, *ibid.* **31**, 488 (1985).

<sup>12</sup>W. P. Alford, R. L. Helmer, R. Abegg, A. Celler, O. Häusser, K. Hicks, K. P. Jackson, C. A. Miller, S. Yen, R. E. Azuma, D. Frekers, R. S. Henderson, H. Baer, and C. D. Zafiratos, *Phys. Lett. B* **179**, 20 (1986).

<sup>13</sup>(a) N. Auerbach and A. Klein, *Nucl. Phys.* **A395**, 77 (1983); (b) *Phys. Rev. C* **30**, 1032 (1984).

<sup>14</sup>R. L. Helmer, *Can. J. Phys.* **65**, 588 (1987).

<sup>15</sup>S. Yen, B. M. Spicer, M. A. Moinester, K. Raywood, R. Abegg, W. P. Alford, A. Celler, T. E. Drake, D. Frekers, O.

Häusser, R. L. Helmer, R. S. Henderson, K. H. Hicks, K. P. Jackson, R. Jeppesen, J. D. King, N. S. P. King, K. Lin, S. Long, C. A. Miller, V. C. Officer, R. Schubank, G. G. Shute, M. C. Vetterli, and A. I. Yavin, *Phys. Lett. B* **206**, 597 (1988).

<sup>16</sup>M. A. Moinester, A. Trudel, K. Raywood, S. Yen, B. M. Spicer, R. Abegg, W. P. Alford, N. Auerbach, A. Celler, D. Frekers, O. Häusser, R. L. Helmer, R. S. Henderson, K. H. Hicks, K. P. Jackson, R. G. Jeppesen, N. S. P. King, S. Long, C. A. Miller, M. C. Vetterli, J. Watson, and A. I. Yavin, *Phys. Lett. B* **230**, 41 (1989).

<sup>17</sup>J. Wambach, S. Drozd, A. Schulte, and J. Speth, *Phys. Rev. C* **37**, 1322 (1988); private communication.

<sup>18</sup>A. Klein, W. G. Love, and N. Auerbach, *Phys. Rev. C* **31**, 710 (1985); private communication.

<sup>19</sup>M. Yabe, *Phys. Rev. C* **36**, 858 (1987).

<sup>20</sup>M. A. Moinester, *Can. J. Phys.* **65**, 660 (1987).

<sup>21</sup>R. S. Henderson, W. P. Alford, D. Frekers, O. Häusser, R. L. Helmer, K. H. Hicks, K. P. Jackson, C. A. Miller, M. C. Vetterli, and S. Yen, *Nucl. Instrum. Methods* **A257**, 97 (1987).

<sup>22</sup>E. Segre, *Nuclei and Particles*, 2nd ed. (Benjamin, New York, 1977), pp. 48-50.

<sup>23</sup>J. F. Janni, *At. Data Nucl. Data Tables* **27**, 341 (1982).

<sup>24</sup>R. A. Arndt and L. D. Soper, *Scattering Analysis Interactive Dial-in (SAID) program*, 1987, unpublished.

<sup>25</sup>F. Osterfeld, *Phys. Rev. C* **26**, 762 (1982).

<sup>26</sup>F. Osterfeld, D. Cha, and J. Speth, *Phys. Rev. C* **31**, 372 (1985).

<sup>27</sup>G. M. Crawley, N. Anantaraman, A. Galonsky, C. Djalali, N. Marty, M. Morlet, A. Willis, J.-C. Jourdain, and P. Kitching,

- Phys. Rev. C **26**, 87 (1982).
- <sup>28</sup>P. Schwandt, H. O. Meyer, W. W. Jacobs, A. D. Bacher, S. E. Vigdor, M. D. Kaitchuck, and T. R. Donoghue, Phys. Rev. C **26**, 55 (1982).
- <sup>29</sup>J. Rapaport, J. D. Carlson, D. E. Bainum, T. S. Cheema, and R. W. Finlay, Nucl. Phys. **A286**, 232 (1977).
- <sup>30</sup>B. A. Brown and A. Trudel, private communication.
- <sup>31</sup>R. Schaeffer and J. Raynal, Program DWBA70 (unpublished); J. R. Comfort, extended version DW81 (unpublished).
- <sup>32</sup>H. V. von Geramb, in *The Interaction between Medium Energy Nucleons in Nuclei, (Indiana Cyclotron Facility, Bloomington, Indiana)*, Proceedings of the Workshop on the Interactions Between Medium Energy Nucleons in Nuclei, AIP Conf. Proc. No. 97, edited by H. O. Meyer (AIP, New York, 1983), p. 44.
- <sup>33</sup>M. Lacombe, B. Loiseau, J. M. Richard, R. Vinh Mau, J. Cote, P. Pires, and R. de Tourriel, Phys. Rev. C **21**, 861 (1980).
- <sup>34</sup>R. D. Smith and J. Wambach, Phys. Rev. C **36**, 2704 (1987); private communication.
- <sup>35</sup>S. D. Bloom, G. J. Mathews, and J. A. Becker, Can. J. Phys. **65**, 684 (1987).
- <sup>36</sup>N. Auerbach, A. Klein, and W. G. Love, in *Antinucleon- and Nucleon-Nucleus Interactions*, edited by G. E. Walker, C. D. Goodman, and C. Olmer (Plenum, New York, 1985), p. 323.
- <sup>37</sup>T. N. Taddeucci, C. A. Goulding, T. A. Carey, R. C. Byrd, C. D. Goodman, C. Gaarde, J. Larsen, D. Horen, J. Rapaport, and E. Sugarbaker, Nucl. Phys. **A469**, 125 (1987).
- <sup>38</sup>C. D. Goodman, C. A. Goulding, M. B. Greenfield, J. Rapaport, D. E. Bainum, C. C. Foster, W. G. Love, and F. Petrovich, Phys. Rev. Lett. **44**, 1755 (1980).
- <sup>39</sup>V. A. Kuz'min and V. G. Soloviev, Nucl. Phys. **A486**, 118 (1988).
- <sup>40</sup>F. P. Brady, T. D. Ford, J. L. Romero, C. M. Castaneda, J. R. Drummond, E. L. Hjort, N. S. P. King, B. McEachern, D. S. Sorenson, Zin Aung, A. Klein, W. G. Love, and J. K. Wambach, Phys. Rev. C **40**, 475 (1989).
- <sup>41</sup>F. A. Gareev, Yu. A. Glukhov, S. A. Goncharov, V. V. Danichev, A. S. Dem'yanova, S. N. Ershov, G. S. Kazacha, A. A. Ogloblin, N. I. Pyatov, S. B. Sakuta, and S. A. Fayans, Yad. Fiz. **48**, 1217 (1988) [Sov. J. Nucl. Phys. **48**, 773 (1988)].